ISSN 1330-3651 (Print), ISSN 1848-6339 (Online)
UDC/UDK 629.735.015.3:533.6.013

HYBRID APPROACH IN THE INITIAL AERODYNAMIC, STABILITY AND PERFORMANCE CALCULATIONS OF A LIGHT AIRPLANE

Ivan Kostić, Zoran Stefanović, Zlatko Petrović, Olivera Kostić, Abdulhakim Essari

Original scientific paper
The paper is focused on the preliminary aerodynamic analyses of a new light aircraft in symmetrical flight configurations. Initial calculations have been done using a 3D vortex lattice method. Since this method is based on inviscid flow concept, the non-linear calibration diagrams for the effectiveness and circulation of control surfaces have been derived from wind tunnel test data of an existing airplane. These calibration functions have been interpolated for a new light aircraft geometry, and analyses of lift and moment coefficients with different flaps and elevator deflections have been performed. Deflected flaps and elevator generate local lift redistributions which contribute to the induced drag, even at angles of attack when the total airplane lift is zero, which has been successfully determined by the applied CFD model. Parasite drag components, omitted by CFD calculations, have been obtained using DVL and Datcom methods and superimposed with CFD results, giving complete new aircraft polars, which have been successfully applied in longitudinal stability and basic performance estimates.

Keywords: *aerodynamics, hybrid method, light aircraft, stability and performance, symmetrical flight conditions*

Hibridni pristup u inicijalnim proračunima aerodinamike, stabilnosti i performansi lakog zrakoplova

Izvorni znanstveni članak
Rad je fokusiran na preliminarne aerodinamične analize novog lakog zrakoplova u simetričnim slučajevima leta. Inicijalni proračuni urađeni su pomoću 3D metode vrtložne rešetke. Pošto se ova metoda bazira na konceptu neviskoznog fluida, nelinearni kalibracijski dijagrami za efikasnost i cirkulaciju upravljačkih površina određeni su na osnovu aerotunelskih ispitivanja jednog postojećeg zrakoplova. Ove funkcije su zatim interpolirane za geometriju novog lakog zrakoplova i izvršene su analize koeficijenata uzgona i momenta za različite kombinacije otklona krilaca i kormila visine. Otklonjena krilca i kormilo visine generiraju lokalne redistribucije uzgona koje doprinose induciranom otporu, čak i pri napadnim kutovima pri kojima je ukupni uzgon zrakoplova jednak nuli, i takav induciran otpor konfiguracije uspješno je određen primijenjenim CFD modelom. Komponente parazitnog otpora koje CFD proračun izostavlja, određene su metodama DVL i Datcom i superponirane sa CFD rezultatima, čime su dobivene kompletne polare novog zrakoplova, koje su uspješno primijenjene u procjenama značajki uzdužne stabilnosti i osnovnih performansi.

Ključne riječi: *aerodinamika, hibridna metoda, laki zrakoplov, simetrični slučajevi leta, stabilnost i performanse*

1 Introduction

Proper estimates of aerodynamic characteristics are essential for the fulfillment of the assigned flying and technical requirements, even in the early stages of a new airplane design. It is necessary to investigate at least several possible design options, and efficiently converge to the most promising one. So the preliminary aerodynamic analyses should be quick, efficient and reliable. This paper describes the methodology applied within that stage of aerodynamic analysis of a new light trainer aircraft (NLA - Fig. 1).

At the initial computational analyses, the authors have used a fairly simple CFD model based on 3D vortex lattice method (VLM). Such inviscid calculation model [1, 2] inherently neglects boundary layer influence and separation effects, so the effectiveness of the flaps and control surfaces are overestimated at moderate and higher deflection angles, and parasite drag components cannot be determined. The lift and moment curves can be obtained only in their linear domains, and just the induced drag polars can be calculated. In order to overcome these problems and obtain complete final diagrams, the authors have applied a hybrid method approach, developed in two directions:

(I) In order to obtain proper effectiveness of flaps and control surfaces within the CFD calculations, the non-linear calibration factors have been successfully derived from wind tunnel test data of the light airplane Utva 75, which has been in operation for several decades, both as military and civilian primary trainer (this airplane is still in use in Serbia, other ex-Yugoslav republics and several countries around the world). The calibration factors were then recalculated for the NLA's design geometry, including the additional circulation correction parameters, which take into account the different lifting characteristics and influences of applied slotted flaps, instead of the plane flaps simulated by VLM.

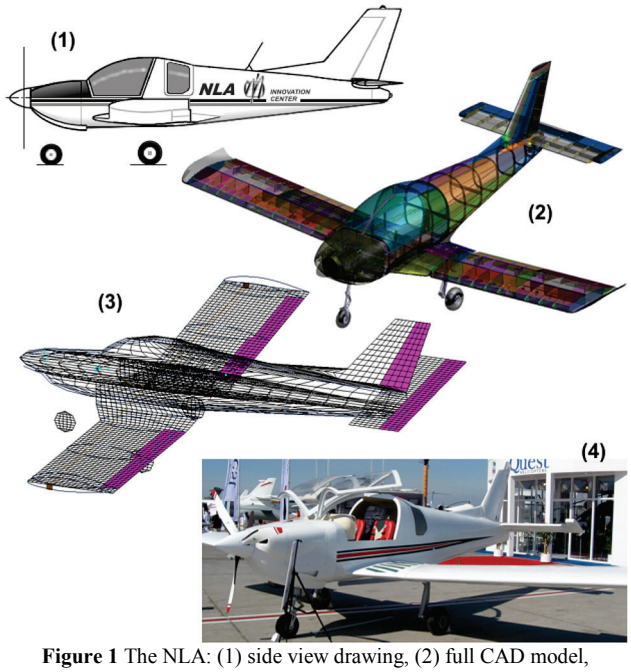

Figure 1 The NLA: (1) side view drawing, (2) full CAD model, (3) 3D model used for vortex lattice calculations, and (4) completely equipped full size airplane mockup

(II) The parasite drag components, which cannot be obtained by the applied CFD calculations, were determined using reliable analytical and semi-empirical methods. These results have been superimposed with the induced drag values, which VLM successfully calculates for many combinations of flaps and elevator deflections, and angles of attack, which analytical methods can hardly quickly estimate to such level of accuracy.

Results from stages (I) and (II) have enabled predictions of the most important aerodynamic, longitudinal stability and performance characteristics, necessary for evaluation of the design in its early development stages.

2 Determination of calibration functions

In order to obtain calibration factors for the NLA's elevator and flaps effectiveness and circulation, initially the 3D CFD model of Utva 75 has been generated, fully compatible with the model of NLA from Fig. 1 - (3), considering the paneling patterns and numbers. The VLM analyses of Utva 75 have been performed for the symmetrical flow cases (angle of attack variations, without and with different combinations of elevator and flaps deflections, without sideslip and aileron or rudder deflections) as those performed in wind tunnel tests of this airplane [3].

2.1 Notes on vortex lattice calculations

In vortex lattice methods, an airplane is initially segmented into a system of panels. The paneling scheme used for here presented calculations is shown in Fig. 1. Each n-th panel is represented by a horseshoe vortex of strength Γ_n (which consists of a bound vortex positioned at the quarter panel chord position, and two semi-infinite trailing vortices), by the control point at 3/4 of the panel chord at its mid section, and appropriate normal vector $\boldsymbol{n}$ (Fig. 2).

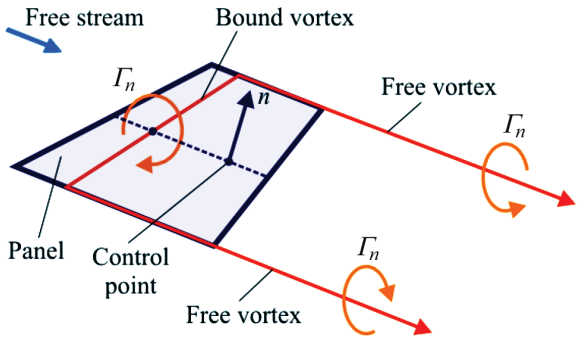

Figure 2 Each panel is represented by a horseshoe vortex, a control point, and a normal vector

The velocities induced by all horseshoe vortices in a control point of a given panel are calculated using the law of Biot-Savart [1, 2]. The summation is performed for all control points, and a set of linear algebraic equations for the calculation of horseshoe vortex strengths is generated. Their Γ_n values are determined by satisfying the boundary condition of "no flow through the surface", i.e. that the total velocity component (free stream plus induced) in the direction of normal vector $\boldsymbol{n}$ must be equal to zero for each of the panels.

Although the applied vortex lattice method is based on the planar *presentation* of the airplane configuration, the influence of actual mean surface cambers, incidences, dihedral and twist angles, deflections of control surfaces and flaps, must be taken into account. For example, coordinates of NACA 65_2-415 airfoil [4] for Utva's wing had to be assigned, while for fuselage, its side shape had to be defined (see Fig. 3).

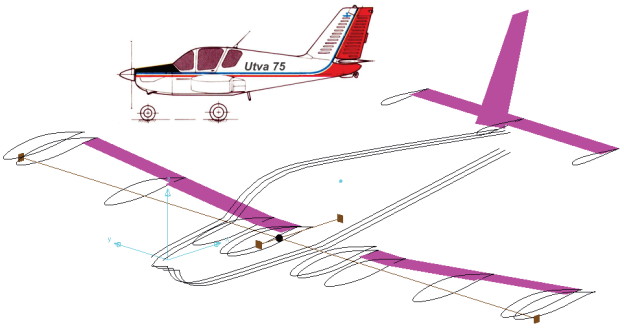

Figure 3 Cambers and control surfaces which define normal vectors

The vortex strengths are related to the lifting surface circulation, and the pressure differential between the upper and lower surface side pressure coefficients $\Delta C_P = C_{PU} - C_{PL}$ (according to here applied convention, as shown in Fig. 4).

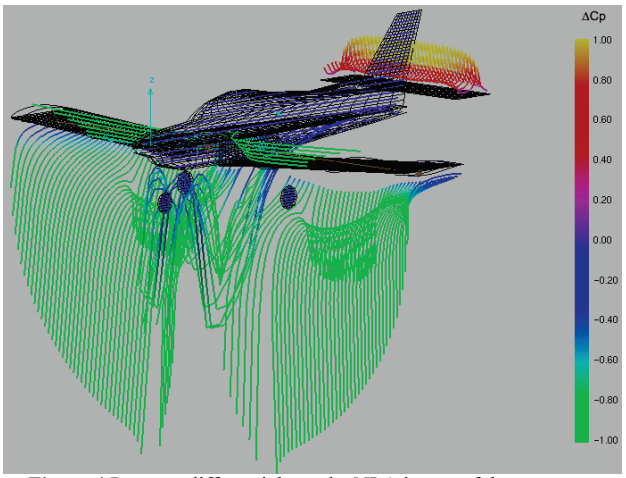

Figure 4 Pressure differentials on the NLA in one of the test cases

2.2 Elevator and flaps calibration parameters

The angle of attack α_f, which is defined with respect to the fuselage reference axis, has been varied in the range of $\alpha_f = -12° \div +10°$. The VLM is based on the potential flow model, so both C_L and C_M curves can be calculated only in linear domains, and angles $\alpha_f > +10°$ have not been considered. Initially, with zero flaps and elevator deflections, the results obtained by VLM have shown good agreements for the slopes of C_L and C_M curves, but both functions were shifted with respect to the wind tunnel points. So the first calibration parameters that were considered for VLM were the incidences. Incidence corrections of +0,9° for the wing and +2,0° for the tail have given very good match between wind tunnel and VLM results, and they have been preserved and applied in

all other VLM Utva 75 analyses. (The most probable cause for this correction is that the wind tunnel model, tested in 1976, did not have the same wing and tail incidence angles as the production airplanes later on, +2,0° on the wing and −2,0° on tail; this information is not given in [3]).

In the next step, with zero flaps deflection, the elevator deflections were varied in range $\delta_e = -30°$ (up) ÷ +20° (down), with 10° increments. In this case slopes were also good, but shifts, especially of moment curves, were quite large (example is given in Fig. 5). The attempt to apply some generalized corrections for effectiveness, such as suggested in [4], did not give any satisfactory matches with wind tunnel data.

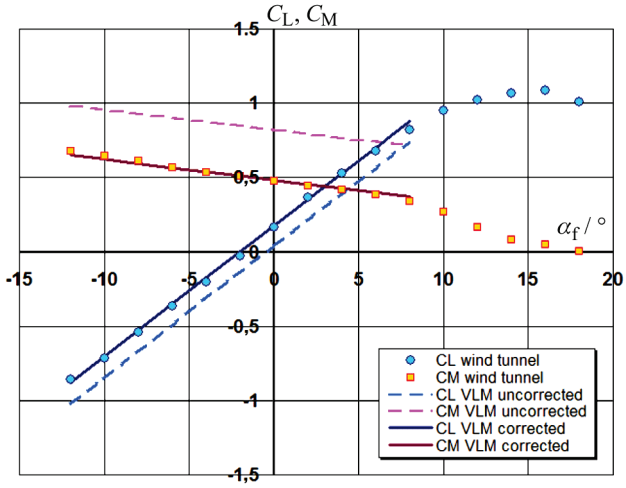

Figure 5 Utva 75 wind tunnel data and VLM results, with zero flap deflection and elevator deflection $\delta_e = -30°$ (η_e calibration)

After numerous VLM test runs, the values of elevator effectiveness calibration factor η_e, which provided good match with wind tunnel were η_e = 0,6; 0,75; 0,9; 1,0; 0,82 and 0,7 respectively, for the above mentioned δ_e range, being a non-linear and asymmetrical function with respect to zero elevator deflection.

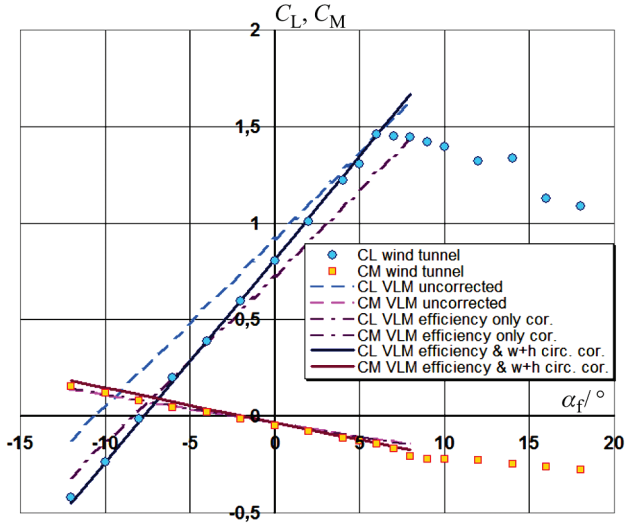

Figure 6 Utva 75 wind tunnel data and VLM results, $\tau = 25°$, $\delta_e = 0°$ (calibrations of η_f, $Cirw_f$, $Cirh_f$)

The following VLM analyses were performed for flaps deflections of $\tau = 25°$ and $\tau = 45°$ (values applied in wind tunnel tests), initially without elevator deflection. Uncorrected VLM results for C_M were quite good, but C_L showed both gradient and shift discrepancies (Fig. 6). In this case, the problem was more complicated, because both Utva 75 and NLA have the so called "single slotted" flaps. Such flaps increase airfoil lift due to two principal effects [7]: (a) increased camber, proportional to deflection angle, and (b) when deflected, a convergent gap between the wing structure and flap (which does not exist in case of "plain" flaps) accelerates the air from lower wing camber to upper flap surface. This gives additional energy to the boundary layer, and keeps flow better attached to flap surface than in case of plain flaps, thus producing more lift for the same deflection angle. On the other hand, the VLM treats all deflected surfaces as plain flaps. Because of that, beside the flaps effectiveness η_f calibration, the additional lift due to flaps type had to be taken into account by introducing the wing circulation $Cirw_f$ calibration factor (lift force, in physical sense, is modeled by circulation in mathematical sense).

After a number of VLM tests, proper combinations of flaps efficiency η_f factor (affecting shift) and circulation calibration $Cirw_f$ factor (affecting slope) have been defined, which has given very good agreements with experiment. The "fine tuning" of C_M also required the introduction of the third parameter, the horizontal tail circulation calibration $Cirh_f$ due to flaps deflection which, combined with other two, gave precise agreements considering the longitudinal stability derivatives. These values are shown in Tab. 1.

Then, VLM tests with flaps deflected have also been repeated for all elevator deflections, and η_e values for τ = 25° and τ = 45° have been successfully determined. All elevator calibration values are summarized in Tab. 2.

Table 1 Calibrations due to flaps deflections

Utva 75			
τ	η_f	$Cirw_f$	$Cirh_f$
0°	1,00	1,00	1,00
25°	0,64	1,25	1,16
45°	0,52	1,32	1,20

Table 2 Elevator effectiveness calibrations

Utva 75	τ = 0°	τ = 25°	τ = 45°
δ_e	η_e	η_e	η_e
−30°	0,60	0,56	0,52
−20°	0,75	0,68	0,60
−10°	0,90	0,81	0,71
0°	1,00	1,00	1,00
+10°	0,82	0,89	0,94
+20°	0,70	0,77	0,82

Using values from Tabs. 1 and 2, the calibration diagrams for Utva 75 have been drawn (Fig. 7).

Recalculation of NLA's elevator effectiveness has been performed in several steps. It should be noted that this was just one of possible approaches for that purpose, considered quite sufficiently good for the VLM analyses:

(1) It has been assumed that for τ = 0° case, η_e values for Utva 75 and NLA are the same, for the preliminary analysis purposes (in actual design, the NLA' s elevator hinge overhang and horn balances is of the same type as on Utva, typical for many light aircraft; moderate

differences in elevator distances from CG and elevator span sizes of the two airplanes have been neglected).

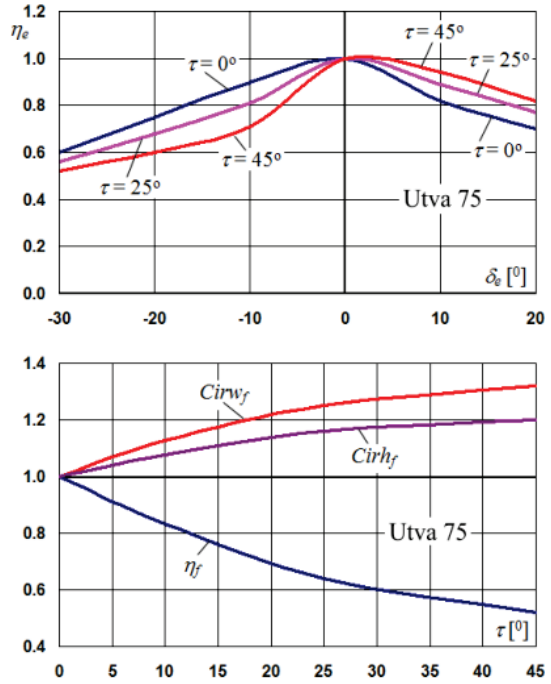

Figure 7 The VLM calibration diagrams for Utva 75, derived from the wind tunnel tests

(2) Differences "$\Delta\eta_{e\,U75}$" between Utva's η_e values for $\tau = 0°$ and the corresponding values for flaps deflected to $\tau = 25°$ and $\tau = 45°$, using data from Tab. 2, have been calculated.

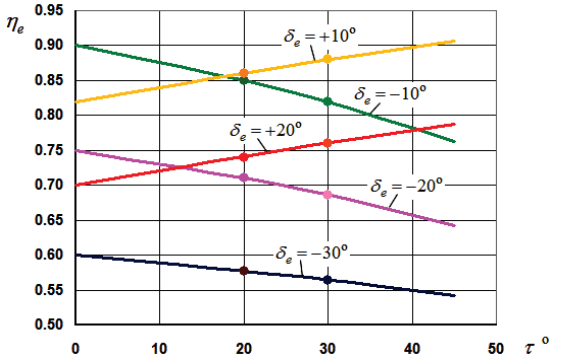

Figure 8 Graphical interpolation of NLA's η_e for $\tau = 20°$ and $\tau = 30°$

(3) Ratios of wing areas in flaps domain versus total wing areas, for the NLA and Utva 75 are $(S_f/S)_{NLA} = 0{,}34$ and $(S_f/S)_{U75} = 0{,}47$, respectively. The ratio of these two values, $(S_f/S)_{RAT} = 0{,}723$ has been applied as scaling factor on $\Delta\eta_{e\,U75}$ values, to obtain corresponding values $\Delta\eta_{e\,NLA}$ for the new light aircraft, with hypothetic flaps deflections $\tau = 25°$ and $\tau = 45°$, and appropriate graphs for $\eta_{e\,NLA}$ have been drawn (Fig. 8)

(4) Since $\eta_{e\,NLA}$ are not linear functions, the NLA's η_e calibrations for its actual flaps deflection angles $\tau = 20°$ and $\tau = 30°$ have been determined by graphical interpolation (also see Fig. 8).

Since both airplanes have single slotted flaps with the same relative chord ratios and kinematics, flaps efficiency calibrations η_f for Utva 75 have been directly applied on the NLA. On the other hand, the Utva's calibrations $Cirw_f$ and $Cirh_f$ had to be scaled by $(S_f/S)_{RAT} = 0{,}723$ (using principally the same logic as previously explained) to calculate the corresponding values for the NLA.

Obtained calibration parameters for the NLA are presented in Tabs. 3 and 4, and in Fig. 9.

Table 3 Calibrations due to flaps deflections

NLA			
τ	η_f	$Cirw_f$	$Cirh_f$
0°	1,000	1,000	1,000
20°	0,700	1,150	1,100
30°	0,590	1,200	1,125

Table 4 Elevator effectiveness calibrations

NLA	$\tau = 0°$	$\tau = 20°$	$\tau = 30°$
δ_e	η_e	η_e	η_e
−30°	0,600	0,577	0,564
−20°	0,750	0,710	0,686
−10°	0,900	0,850	0,816
0°	1,000	1,000	1,000
+10°	0,820	0,860	0,880
+20°	0,700	0,740	0,760

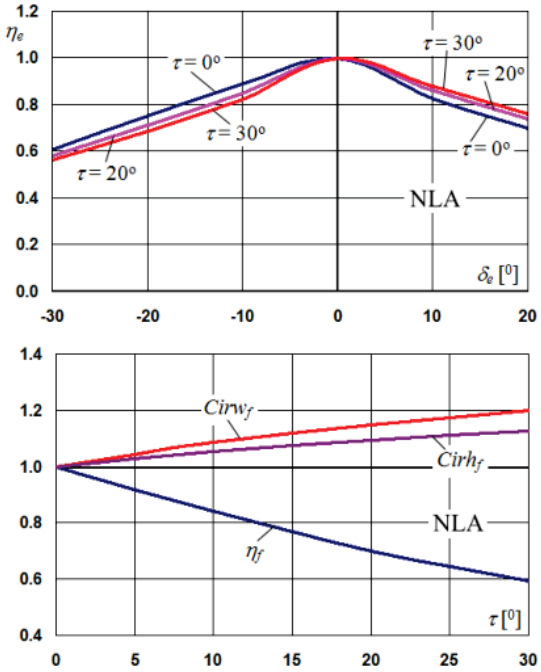

Figure 9 Calibration diagrams derived for the NLA

3 Preliminary evaluations of aerodynamic, stability and performance characteristics of the NLA

After determination of calibration factors for the new light aircraft, it was necessary to perform their verification. In order to do that, the independent calculations for several typical cases have been done by VLM (limited to linear domains of lift and moment coefficients), and by highly recognized Datcom method [8], and very satisfactory agreements have been achieved (several examples are given in [5], and in Fig. 17).

The initial step in the application of VLM analyses of the new light aircraft was the determination of linear domains of lift coefficient C_L and pitching moment coefficients C_M. Three flaps positions $\tau = 0°$, $\tau = 20°$ and $\tau = 30°$ (maximum deflection considered at the time) have been analyzed for elevator deflections in the range δ_e =

−30° to δ_e = +20° with 10° deflection steps. Examples for retracted and fully extended flaps are given in Fig's 10 and 11.

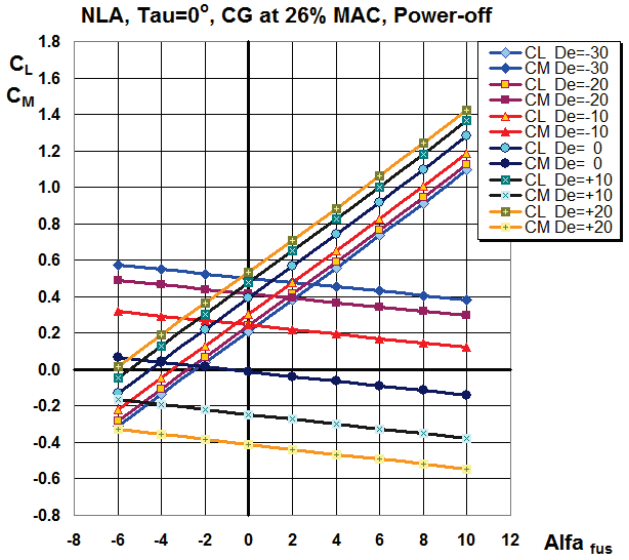

Figure 10 VLM lift and moment coefficients for different δ_e and τ = 0°

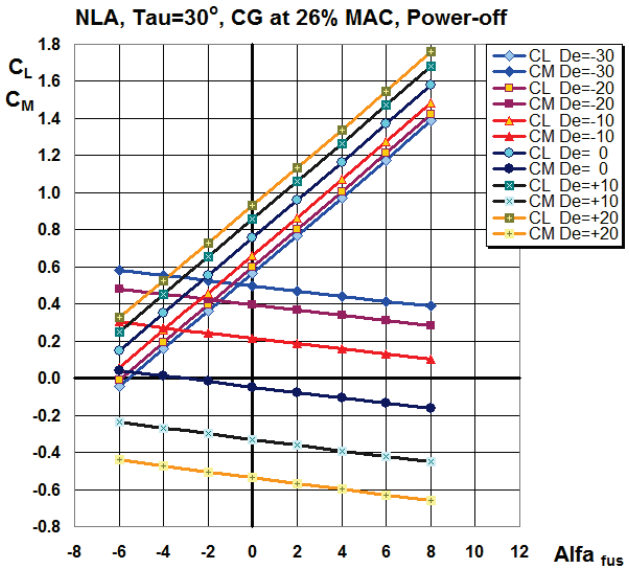

Figure 11 VLM lift and moment coefficients for different δ_e and τ = 30°

These analyses have enabled the generation of $C_L - C_M$ diagrams, where their slopes define the derivative dC_M/dC_L, which represents measure of the airplane's longitudinal static stability (airplane is stable when $dC_M/dC_L < 0$). Since here applied fairly simple VLM method, aimed for preliminary analyses, cannot simulate propeller influences, the obtained longitudinal stability values correspond to the so called "power-off" case.

Additional power plant influences for minimum, cruising and full power on stability have been estimated using semiempirical approach described in [9] and [10], where these influences, obtained from flight tests for different airplane categories, have been superimposed to power-off case results.

Figs. 12 and 13 show curves obtained for τ = 0° and τ = 30° and different elevator deflections, where solid dotted lines represent VLM results. Power-off results are also summarized in Tab. 5, for three characteristic flaps positions, in range of two maximum elevator deflections. (For an airplane whose longitudinal static stability is, for example dC_M/dC_L = −0,1376, it is usually said that it is 13,76 % stable, and such nomenclature is applied in this table.).

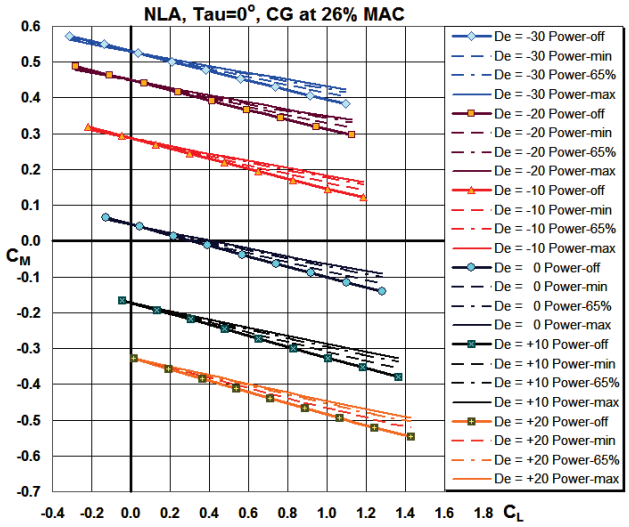

Figure 12 Longitudinal stability diagrams for different δ_e and τ = 0°

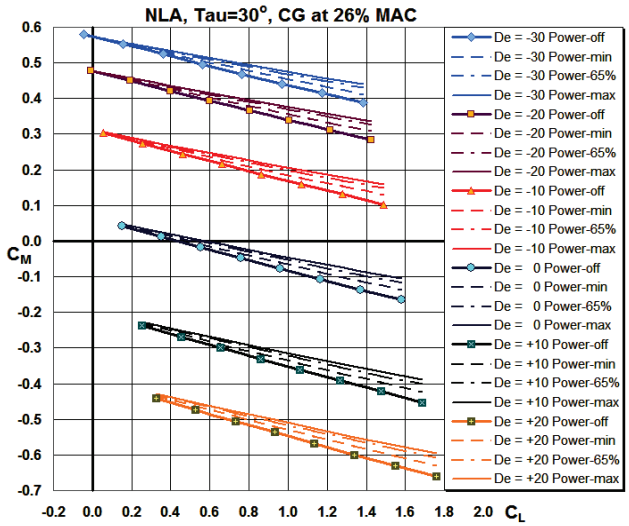

Figure 13 Longitudinal stability diagrams for different δ_e and τ = 30°

Table 5 Longitudinal static stability obtained by VLM (power-off)

Flaps deflection	Longitudinal static stability for elevator deflections in range δ_e = −30° ÷ +20°
τ = 0°	13,76 ÷ 15,85 %
τ = 20°	13,77 ÷ 15,81 %
τ = 30°	13,61 ÷ 15,64 %

The NLA has been considered both as the Utility and Aerobatic category airplane (the difference being in maximum take-off mass MTOM and the corresponding maximum load factor values), so it has powerful elevator, with chord ratio c_e/c_t = 0,4 (ratio between elevator and whole horizontal tail chord). Previous diagrams indicate two important conclusions, drawn from VLM:

(a) The elevator deflection has quite remarkable influence on the airplane's lift coefficient curves, while in some preliminary analytical methods such influence is neglected.

(b) Theoretical analyses generally state that the elevator deflection has no practical influence on longitudinal stability. From Tab. 5 it is obvious that this influence is of the order of 2 %, which definitely is a small influence, but not quite negligible.

Considering analytical drag calculations, a general formula which describes total airplane drag polar can be written as [11]:

$$C_{\mathrm{D}} = C_{\mathrm{D\,min}} + k \cdot C_{\mathrm{L}}^2 + C_{\mathrm{Di}} \tag{1}$$

and often, the second and third member are grouped as:

$$C_{\mathrm{D}} = C_{\mathrm{D\,min}} + \frac{C_{\mathrm{L}}^2}{\pi \cdot AR \cdot e}, \tag{2}$$

where e represents the Oswald's efficiency factor and for the purpose of here presented calculations, we shall use its initial form.

The first two members on the right side of (1) define the parasite drag, not generated by lift. The $C_{\mathrm{D\,min}}$ represents its minimum value for the entire airplane, while $k \cdot C_{\mathrm{L}}^2$ represents its "position" component, dependant on the angle of attack (and for the ease of calculations, it is formally expressed in terms of the lift coefficient).

The third member C_{Di} represents the lift-induced drag, and only this component can be calculated by VLM, because the first two are the consequence of viscous effects.

Theory often treats the induced drag of the wing as the only relevant component contributing to it, defined as:

$$C_{\mathrm{Di}} = \frac{C_{\mathrm{L}}^2}{\pi \cdot AR \cdot (u \cdot s)}, \tag{3}$$

where AR represents the wing's aspect ratio ("relative" wing span), u is the correction for non-elliptical wing planform shape, and s defines the influence of fuselage on induced drag. Taking (3) literally, when lift coefficient is equal to zero, the induced drag does not exist, which is acceptable for simple analytical preliminary calculations.

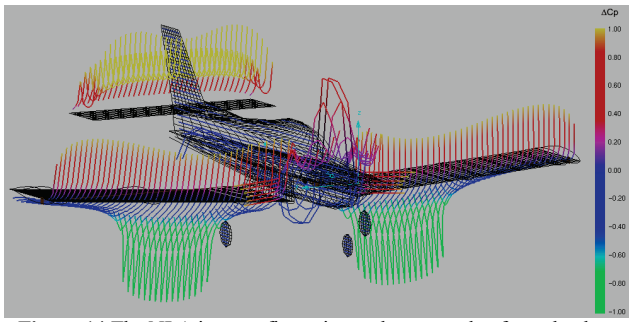

Figure 14 The NLA in a configuration and at an angle of attack when the total airplane's lift is zero, but the induced drag is not

On the other hand, this is not quite true. Namely, with flaps and elevator deflected, the total lift of the entire airplane configuration at a certain angle of attack will be zero, but induced drag will not, since the local lift distributions around lifting surfaces, flaps and elevator will generate local lift-induced drags, and thus $C_{\mathrm{Di}} \neq 0$.

An example is given in Fig. 14 where, at fuselage angle of attack $\alpha_{\mathrm{fus}} = -5{,}6°$, with flaps deflected to $\tau = 30°$ and elevator deflection $\delta_{\mathrm{e}} = -30°$, lift coefficient of the NLA is $C_{\mathrm{L}} = 0$, while $C_{\mathrm{Di}} = 0{,}0469 \neq 0$.

The capability of VLM to calculate the actual induced drag for any given configuration presents a great advantage over analytical methods (certainly, to a level expected in preliminary design studies). Because of that, for aerodynamic calculations of the NLA, a hybrid method approach has been applied. The first two members in (1) have been determined by reliable analytical methods, while the induced drag has been calculated by VLM:

$$C_{\mathrm{D}} = \left(C_{\mathrm{D\,min}} + k \cdot C_{\mathrm{L}}^2\right)_{\mathrm{analytical}} + \left(C_{\mathrm{Di}}\right)_{\mathrm{VLM}}. \tag{4}$$

The value of NLA's minimum drag coefficient $C_{\mathrm{D\,min}} = 0{,}03737$, without flaps and elevator deflections, has been determined using Datcom [8]. The increase of the minimum drag coefficient due to flaps deflections was calculated by DVL method (referenced and described in [7]), giving $\Delta C_{\mathrm{D\,min}} = 0{,}000748$ for $\tau = 20°$, and $\Delta C_{\mathrm{D\,min}} = 0{,}00413$ for $\tau = 30°$. According to Douglas Aircraft Company [11], the parameter k from (1) is $k = 0{,}38 \cdot C_{\mathrm{D\,min}}$ for airplanes of the classical design, with unswept wings. This way, the general equations for total drag of NLA, with flaps deflections $\tau = 0°$, $\tau = 20°$ and $\tau = 30°$ respectively, have been obtained as:

$$C_{\mathrm{D}} = 0{,}03737 + 0{,}0142 \cdot C_{\mathrm{L}}^2 + \left(C_{\mathrm{Di}}\right)_{\mathrm{VLM}}, \tag{5}$$

$$C_{\mathrm{D}} = 0{,}03812 + 0{,}0145 \cdot C_{\mathrm{L}}^2 + \left(C_{\mathrm{Di}}\right)_{\mathrm{VLM}}, \tag{6}$$

$$C_{\mathrm{D}} = 0{,}04150 + 0{,}0158 \cdot C_{\mathrm{L}}^2 + \left(C_{\mathrm{Di}}\right)_{\mathrm{VLM}}. \tag{7}$$

Induced drag polars calculated by VLM, and total drag polar curves, determined using equations (5) ÷ (7), are shown in Figs. 15 and 16 for two characteristic cases $\tau = 0°$, and $\tau = 30°$. When the total configuration lift is zero, it is obvious that only for the case $\tau = 0°$, and elevator deflections $\delta_{\mathrm{e}} = 0°$, $\delta_{\mathrm{e}} = +10°$ and $\delta_{\mathrm{e}} = +20°$ the induced drag coefficient is $C_{\mathrm{Di}} \approx 0$, while for other cases it can be substantially larger than zero, at $C_{\mathrm{L}} = 0$.

The values of maximum lift coefficients and critical angles of attack had to be determined by Datcom, and complete $C_{\mathrm{L}} - \alpha$ curves for three characteristic flaps deflections (without elevator deflections) are shown in Fig. 17. Results for linear domains, obtained by VLM, are shown in the same figure, and they obviously coincide well with Datcom results.

In order to obtain NLA's polars in analytical form, which was necessary for performance calculations, point-to-point values of total drag have been fitted on $C_{\mathrm{L}}^2 - C_{\mathrm{D}}$ diagrams, where parabolic polars convert to linear functions (see Fig. 18):

$$C_{\mathrm{D}} = A + B \cdot C_{\mathrm{L}}^2 \Rightarrow y = A + B \cdot x. \tag{8}$$

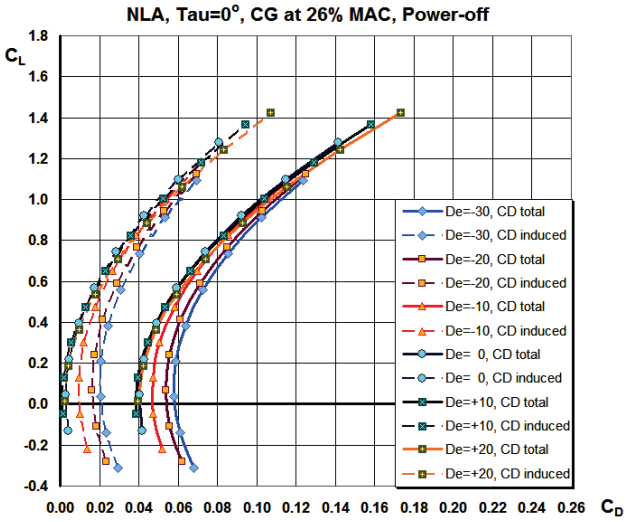

Figure 15 Induced drag (left) and total drag polars (right) for $\tau = 0°$, and different elevator deflections

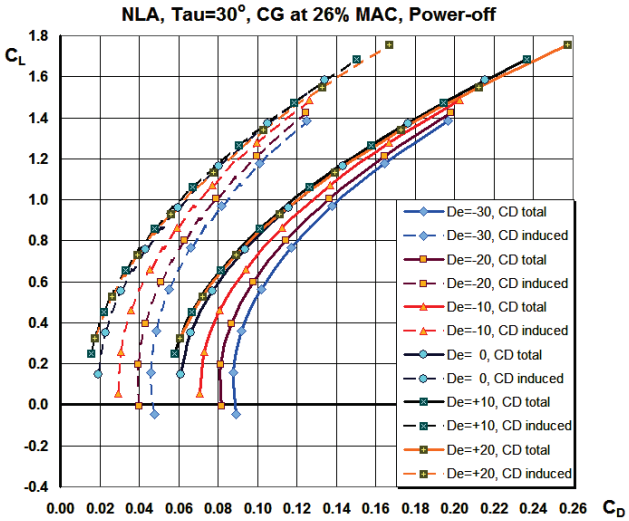

Figure 16 Induced drag (left) and total drag polars (right) for $\tau = 30°$, and different elevator deflections

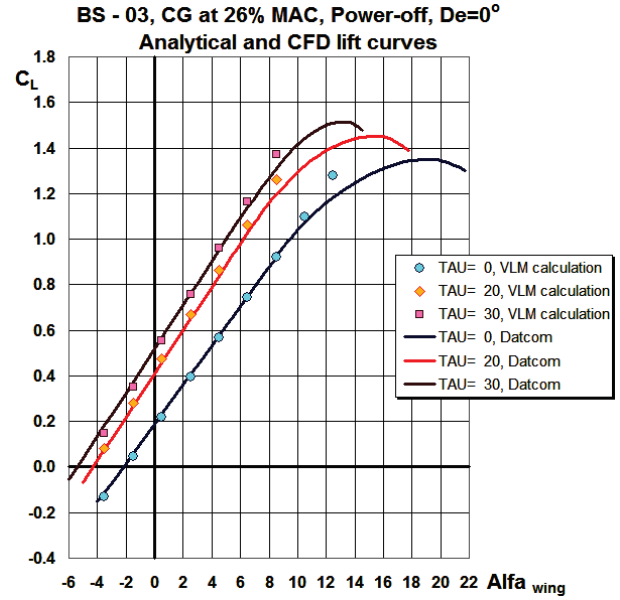

Figure 17 Lift curves obtained by Datcom and VLM, for $\tau = 0°$, $\tau = 20°$ and $\tau = 30°$, without elevator deflection

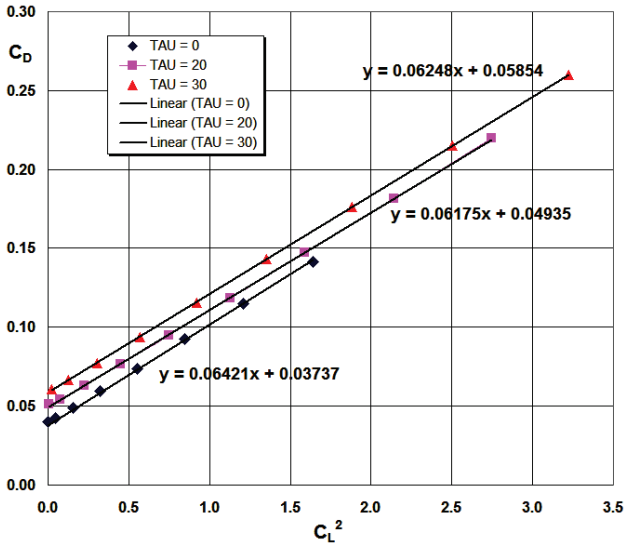

Figure 18 Analytical fitting of drag polars for three flaps positions, without elevator deflections

So the analytical parabolic polars without elevator deflection, for flaps deflections $\tau = 0°$, $\tau = 20°$ and $\tau = 30°$ respectively, have been obtained as:

$$C_{D\,\tau=0} = 0{,}03737 + 0{,}06421 \cdot C_L^2, \tag{9}$$

$$C_{D\,\tau=20} = 0{,}04935 + 0{,}06175 \cdot C_L^2, \tag{10}$$

$$C_{D\,\tau=30} = 0{,}05854 + 0{,}06248 \cdot C_L^2, \tag{11}$$

(all other polars, with elevator deflections, are obtained using the same principle).

At this point it should be emphasized that the equation (2) can be treated as sufficiently accurate only for airplanes in "clean" configurations, i.e. without any control surface deflections, and with not too cambered lifting surfaces. In all other cases [12], it must be written in the form:

$$C_D = C_{D\,\min} + \frac{(C_L - C_{L\,\min,\,drag})^2}{\pi \cdot AR \cdot e}, \tag{12}$$

where $C_{L\,\min,\,drag}$ represents the lift coefficient at which minimum airplane drag is achieved. For practical reasons, since in many cases $C_{L\,\min,\,drag}$ is a proportionally small value, a simplification that $C_L - C_{L\,\min,\,drag} \approx C_L$ can be applied with an acceptable level of accuracy. Then the equation (12) can be written in a simpler form:

$$C_D = C_{D0} + \frac{C_L^2}{\pi \cdot AR \cdot e}, \tag{13}$$

where C_{D0} represents drag at zero-lift coefficient, and it should be kept in mind that generally $C_{D0} \neq C_{D\,\min}$ (more details considering the explanation of this issue can be found in [12], chapter 5).

It means that the NLA's total drag polars (9) ÷ (11), obtained in the previously explained way, actually represent forms of the general equation (13). They are shown in Fig. 19, where calculated values are represented by dots, while fitted polars are shown as solid curves,

extending up to the maximum lift coefficients, defined by Fig. 17.

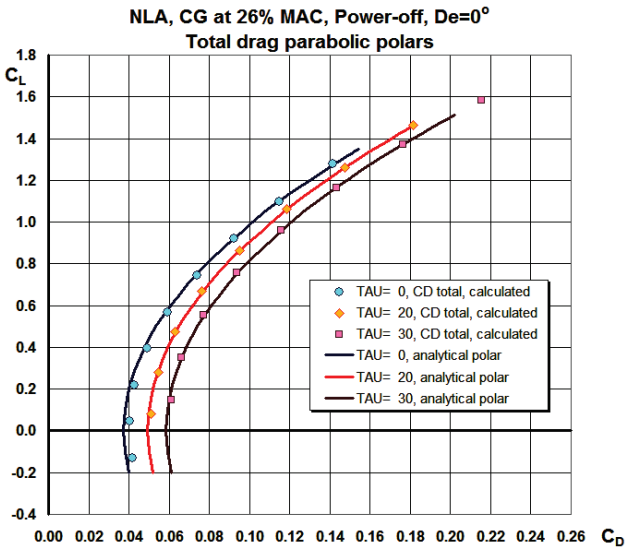

Figure 19 Calculated and fitted analytical parabolic polars of the NLA

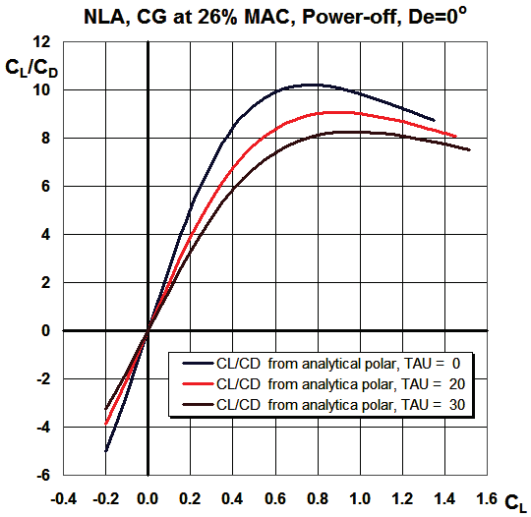

Figure 20 Lift/drag curves for three flaps positions, $\delta_f = 0°$

Using equations (9) ÷ (11), C_L/C_D curves versus C_L have been drawn (Fig. 20).

Manufacturers of many single-engined light airplanes of the NLA's size and category, with metal structures (which is the case with NLA as well), officially state that maximum lift/drag ratios of their airplanes are of the order of $\approx 12 \div 13$ (some examples are given in [12]). On the other hand, many pilots report that, during operational use, maximum C_L/C_D values of these airplanes can hardly exceed values $10 \div 11$. In that sense, obtained estimate of $(C_L/C_D)_{max} = 10{,}21$ at $C_L = 0{,}76$ for the NLA seems to be quite close to real life, for an airplane of such category and design.

Total drag polars in parabolic form are world-wide used in airplane analyses, because they enable quick and efficient preliminary performance analyses. They provide good drag fitting in most of the available C_L domain, except at high lift coefficients, where they underestimate drag, because the influence of massive separation effects is neglected (in this domain the actual drag cannot be expressed as a simple parabolic function). Practical consequence is that, for example - at small speeds, power required for level flight will be slightly underestimated, while maximum rates of climb will be slightly overestimated in the same speed domain (in Figs. 21 and 22, it would roughly be the domain of up to some 20 km/h above the stalling speed).

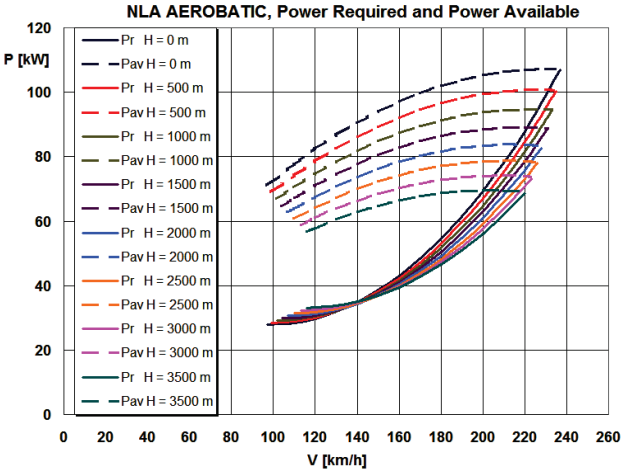

Figure 21 Diagrams of power-required *Pr* and power-available *Pav*

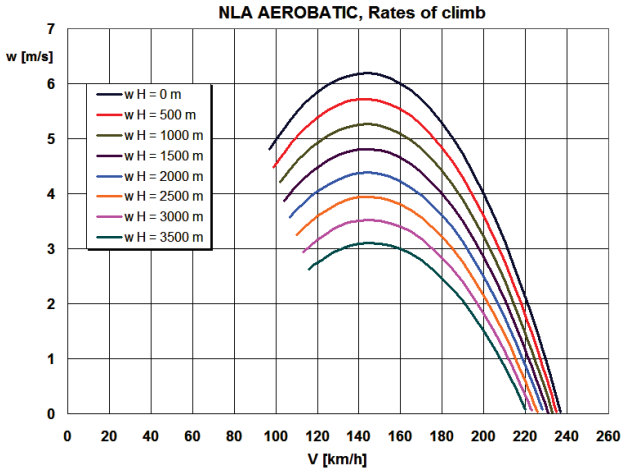

Figure 22 Diagrams of maximum rates of climb at different altitudes

In the initial NLA performance estimates, the two versions have been considered, Aerobatic with MTOM = 920 kg and 150 l of fuel, and Utility, with MTOM = 1000 kg and 250 l of fuel, with 180 HP engine Lycoming IO-360-M1B [13], and initially with two blade 1,93 m diameter, variable pitch - constant speed propeller, manufactured by "MTV-Propeller". Equation (9) has been used for flight performance calculations, while (10) and (11) have been applied in take-off and landing calculations. Since here applied VLM model cannot simulate the ground effects (increase in lift, and decrease in induced drag), the take-off and landing distances contain a small inherent error, which can readily be tolerated for preliminary calculation purposes.

All performance calculations have been done using a Fortran program, custom written by the authors of this paper and based on [9], [10] and [13], with an attempt to achieve optimum compromise between calculations complexity level, time and resource efficiency, and expected accuracy at the preliminary design level (unfortunately, details could not be discussed here, because of the limited scope of the paper). Some of the obtained results are shown in Figs. 21 ÷ 26.

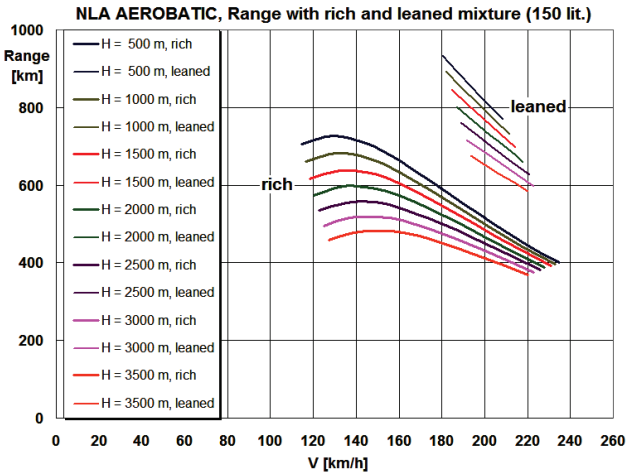

Figure 23 Ranges with full rich, and with leaned mixture

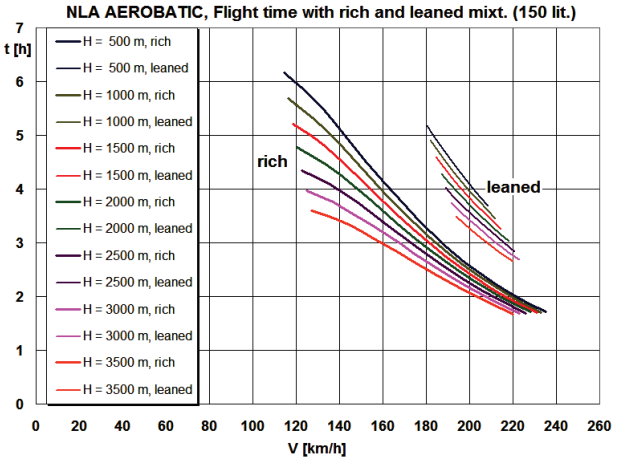

Figure 24 Corresponding flight times with full rich, and leaned mixture

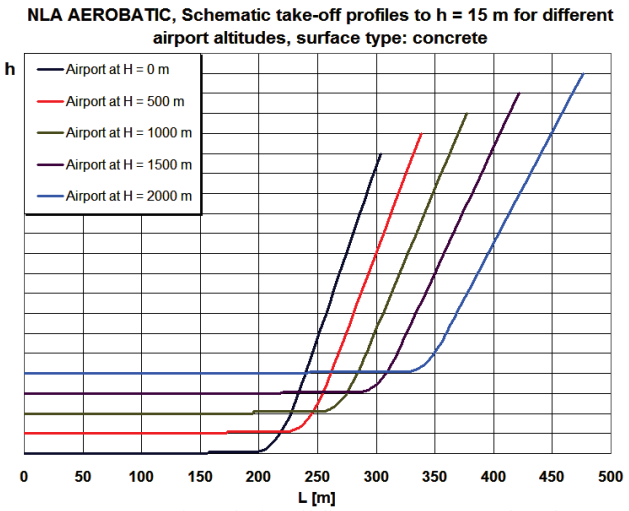

Figure 25 Estimated take-off distances up to 15 m obstacle

In Fig. 23 "range" implies the distance flown in horizontal flight at a given cruising altitude (according to the International Standard Atmosphere ISA), while climb and descend distances are not included. On the selected engine, mixture leaning can be applied only in a limited domain of engine power settings [13], so those curves do not cover complete speed domains, as those for full rich mixture.

The take-off distances (Fig. 25) have been calculated in four phases: (1) accelerated ground roll (integrated in 1 km/h increments), followed by (2) pull-up at $1{,}1 \cdot v_{\text{min TO}}$ and accelerated hold-off flight, theoretically at 0,1 m above terrain, until optimum climb speed is reached, (3) rotation, and (4) steady climb to 15 m.

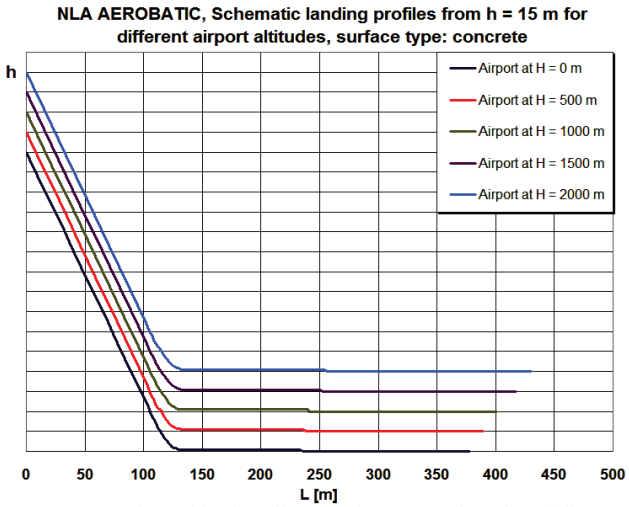

Figure 26 Estimated landing distances from 15 m obstacle to full stop

In the calculation of landing distances, the same logic in reverse order has been applied, starting with steady descent at $1{,}3 \cdot v_{\text{min LAND}}$ and zero thrust assumed, rotation, decelerated level hold-off, touch down at $1{,}15 \cdot v_{\text{min LAND}}$, and decelerated ground roll to full stop.

4 Conclusion

This paper describes the application of a hybrid method approach, which has been used in the preliminary aerodynamic, static stability and performance calculations of a new light aircraft. It involves vortex lattice calculations, experimental wind tunnel data for an airplane of similar category, as well as analytical and semi-empirical calculation methods. In this paper only symmetric flight configurations have been analyzed, with flaps and elevator deflections. Initially, within the vortex lattice method application, the calibrations for effectiveness and circulations of flaps and elevator have been derived from the wind tunnel test data of an existing aircraft of the similar category. This way, reliable induced drag polars have been obtained for the NLA with different combinations of flaps and elevators deflected. The parasite drag components, not calculated by VLM, have been estimated using the well known Datcom and DVL methods. After superimposing the parasite and the induced drag results, the total drag polars and lift/drag ratios have been defined by analytical fitting of point-to-point values, obtained from combined CFD and semi-empirical calculations. Since VLM can calculate moment and lift coefficients only in their linear domains, maximum lift coefficients and critical angles of attack for three characteristic flaps positions have been determined using Datcom. Results have been applied in the stability and performance calculations, based on VLM, analytical and semi-empirical calculation methods, at the complexity levels suitable for preliminary calculations. Described approach has proven to be very efficient in the development of the NLA's geometry and design, within multiple project refinement stages.

5 References

[1] Bertin, J.; Smith, M. Aerodynamics for engineers, Prentice-Hall International Editions, Englewood Cliffs, New Jersey, 1989.
[2] Katz, J.; Plotkin, A. Low Speed Aerodynamics - From Wing Theory to Panel Methods, McGraw-Hill, New York, 1991.
[3] Damljanović, D. Aerodinamička ispitivanja modela aviona Utva-75 u aerotunelu T-35 (Aerodynamic tests of Utva-75 airplane in T-35 wind tunnel), graduate student's seminar work in Aerodynamics II course, University of Belgrade, Faculty of Mechanical Engineering, Belgrade 2009.
[4] Abbott, I. H.; Doenhoff, A. E. Theory of Wing Sections Including a Summary of Airfoil Data, Dover Publications, Inc., New York, 1959.
[5] Stefanović, Z.; Kostić, I.; Kostić, O. Efficient Evaluation of Preliminary Aerodynamic Characteristics of Light Trainer Aircraft. // Engineering Review. 32, 1(2012), pp. 49-56.
[6] Stefanović, Z.; Kostić, I.; Kostić, O. Primary Aerodynamic Analyses of a New Light Aircraft in Symmetrical Flight Configurations. // The 7th International Symposium KOD 2012 / Balatonfüred Hungary, 2012. Proceedings, pp. 97-104.
[7] Stefanović, Z. Aeroprofili (Airfoils), University of Belgrade, Faculty of Mechanical Engineering, Belgrade, 2005.
[8] Ellison, D. E.; Malthan, L. V. et al. USAF Stability and Control DATCOM, Air Force Flight Dynamics Laboratory & Douglas Aircraft Company, Inc, Wright-Patterson Air Force Base, Ohio, 1965/1978.
[9] Perkins, C D.; Hage, R. E. Airplane performance, stability and control, John Wiley & Sons Inc., New York, 1949/1960.
[10] Rendulić, Z. Mehanika leta (Flight mechanics), Vojnoizdavački i novinski centar, Belgrade, 1987.
[11] Shevell, R. S. Fundamentals of flight, Stanford University - Prentice-Hall International Editions, Englewood Cliffs, New Jersey, 1983.
[12] Roscam, J.; Chuan-Tau, E. L. Airplane aerodynamics and performance, DARcorporation, Lawrence, Kansas, 1997.
[13] Operator's Manual Lycoming O-360, HO-360, IO-360, AIO-360, HIO-360 & TIO-360 Series // 8th Edition, Part No. 60297-12, Williamsport, PA., 2005.

Authors' addresses

Ph.D. Ivan Kostić, Associate Professor
University of Belgrade
Faculty of Mechanical Engineering
Kraljice Marije 16
11000 Belgrade, Serbia
+ 381 63 8561639
ikostic@mas.bg.ac.rs

Ph.D. Zoran Stefanović, Full Professor
University of Belgrade
Faculty of Mechanical Engineering
Kraljice Marije 16
11000 Belgrade, Serbia

Ph.D. Zlatko Petrović, Full Professor
University of Belgrade
Faculty of Mechanical Engineering
Kraljice Marije 16
11000 Belgrade, Serbia

M.Sc. Olivera Kostić, Research Assistant
University of Belgrade
Faculty of Mechanical Engineering
Kraljice Marije 16
11000 Belgrade, Serbia

M.Sc. Abdulhakim Essari, Ph.D. student
University of Belgrade
Faculty of Mechanical Engineering
Kraljice Marije 16
11000 Belgrade, Serbia